Advances in Computational & Experimental Engineering & Science

Computation of Incompressible Flows with Immersed Bodies on Unstructured Cartesian Grids

Dartzi Pan[1]

Summary

A simple and effective computational model for the immersed bodies in incompressible flows is implemented on unstructured Cartesian grids. The domain inside the immersed body is viewed as being occupied by the same fluid as outside with a prescribed divergence-free velocity field. The pressure inside the immersed body satisfies the same pressure Poisson equation as outside. The model is implemented in an implicit fractional step pressure correction method. Steady and unsteady flows over a circular cylinder are computed as test problems. An ellipse in "figure-8" motion is computed to demonstrate the capability of the present model to treat complex body movements.

Introduction

Recently numerical methods for solving incompressible flows on non-body-fitted Cartesian grids are gaining popularity for their relative ease in treating complex immersed bodies in the flow field [1-5]. The differences among these methods lie on the different way the boundary conditions for the immersed bodied are enforced. The immersed boundary method [1] and the virtual boundary method [2] simulate the no-slip boundary condition on the body surfaces by adding appropriate momentum forcing terms to the appropriate cells. In Cartesian cut-cell methods [3,4,5], the flow variables for the cut cells are either solved based on the actual shape of the cut cells [3], or interpolated from the surrounding fluid and body cells [4,5] without actually solving the conservation equations for the cell.

In this work, we view the domain inside the solid body as being occupied by the same fluid as outside with a prescribed divergence-free velocity field. In this view a fluid-body interface is similar to a fluid-fluid interface commonly encountered in the Volume of Fluid (VOF) method for the two-fluid flow problems. Since the velocity field inside the body is divergence-free, the pressure inside obeys the same pressure Poisson equation as outside. For the grid cells containing the fluid-body interface, a mixture of the "two fluids" based on the fluid volume is assumed. This volume averaging of the velocity automatically enforces the no-slip boundary condition inside the interface cell, which smears the fluid-body interface to the width of one cell. We have implemented the above model in an implicit fractional step pressure correction method on unstructured

[1] Department of Aeronautics and Astronautics, National Cheng Kung University, Taiwan, ROC

Advances in Computational & Experimental Engineering & Science

Cartesian grid [6,7]. In this paper we show some test results of flows over a stationary circular cylinder and an ellipse in large amplitude "figure-8" flapping motion.

Implicit Fractional Step Pressure Correction Method

The incompressible Navier-Stoked equations are

$$\begin{aligned} \vec{\nabla}\cdot\vec{v} &= 0 \\ \frac{\partial\vec{v}}{\partial t} + \vec{\nabla}\cdot(\vec{v}\vec{v}) - \frac{1}{Re}\nabla^2\vec{v} + \vec{\nabla}P &= 0 \end{aligned} \tag{1}$$

where $\vec{v}$ and P are Cartesian velocity and pressure, Re is Reynolds number. The backward time differencing scheme is used to advance the momentum equations with the pressure fixed at time level n :

$$\frac{c_1\vec{v}^{*} - c_2\vec{v}^{n} + c_3\vec{v}^{n-1}}{Dt} + \vec{R}^{*} + \vec{\nabla}P^{n} = 0 \tag{2}$$

where Δt is the time increment and $\vec{R}^{*}$ represents the convection and the viscous fluxes. The constants are $c_1 = 1.5$, $c_2 = 2$ and $c_3 = 0.5$ for the second-order accurate backward differencing scheme, and $c_1 = 1$, $c_2 = 1$ and $c_3 = 0$ for the first order Euler implicit scheme. The intermediate velocity $\vec{v}^{*}$ generally does not satisfy the divergence-free condition. It is corrected by the following correction step:

$$\vec{v}^{n+1} = \vec{v}^{*} - \Delta t\vec{\nabla}f \tag{3}$$

where $f = P^{n+1} - P^{n}$ is the pressure correction. By requiring $\vec{v}^{n+1}$ be divergence-free, we obtain the Poisson equation for the pressure correction:

$$\nabla^2 f = \frac{\vec{\nabla}\cdot\vec{v}^{*}}{\Delta t} \tag{4}$$

Equations (2), (3) and (4) constitute the implicit fractional step pressure correction method used in this work.

Finite Volume Discretization

A finite volume method based on the integral form of Eq. (1) is used to discretize the momentum equation on a cell-centered unstructured Cartesian grid system. The variable states at the cell faces are linearly reconstructed from the center values. The convection fluxes are upwind oriented based on the velocity at the cell face. The pressure force is computed using the reconstructed pressure state at the cell face, while the viscous fluxes are computed using the velocity gradients at the cell face. Overall, a second order accurate upwind difference scheme is used for the convection fluxes and central

Advances in Computational & Experimental Engineering & Science

difference schemes are used for the pressure and viscous fluxes. To compute the divergence of velocity, a normal face velocity is defined separately from the cell center velocity. A fourth derivative of pressure is added in the divergence field through the normal face velocity. This face velocity is corrected in a similar fashion as Eq. (3), and thus constructing the discretized Poisson equation for the pressure correction.

Treatment of Immersed Body

The position and the velocity $\vec{v}_B$ of the immersed bodies are assumed known from some appropriate governing equations. The volume ratio in a cell occupied by the solid body, f_B, is used to identify the body cells $(f_B=1)$, the fluid cells $(f_B=0)$ and the interface cells $(0<f_B<1)$. The body surface is represented by the contour of $f_B=0.5$. Since the velocity inside the body surface is known, we modify Eq. (2) to

$$(1-f_B)\left(\frac{c_1\vec{v}^{*}-c_2\vec{v}^{n}+c_3\vec{v}^{n-1}}{Dt}+\vec{R}^{*}+\vec{\nabla}P^{n}\right)+f_B\left(\frac{c_1\vec{v}^{*}-c_1\vec{v}_B^{n+1}}{Dt}\right)=0 \tag{5}$$

Equation (5) recovers Eq. (2) for fluid cells, and it yields $\vec{v}^{*}=\vec{v}_B^{n+1}$ for body cells. As for interface cells, the solution of Eq. (5) is a volume-averaged mixture of the body velocity and the velocity computed by the flow conservation. This volume averaging is a simple and effective treatment to account for the effects of the fluid-body interface. Since $\vec{v}_B$ is assumed divergence-free, the Poisson equation with a zero source term is used to compute the pressure correction inside the body. The elliptical nature of the Poisson equation ensures that the pressure field inside the body adjusts itself according to the pressure field outside. The pressure and viscous forces acting on the body are obtained as volume forces by

$$\vec{f}_{Body}=\sum_{cell} f_B\left(-\vec{\nabla}P+\frac{1}{Re}\nabla^2\vec{v}\right)DV \tag{6}$$

Flows over a Stationary Circular Cylinder

The steady and unsteady flows over a circular cylinder of unit diameter at *Re=40* and *200* are computed on an unstructured Cartesian grid. The grid is refined around the cylinder to have about *52* cells across the diameter. The cylinder volume computed by f_B is about *0.3%* less than the true value. The outer boundaries are *20* diameters away from the cylinder. The uniform flow condition is set to the inflow and the two side boundaries. The downstream boundary follows the upwind differenced equation of $(\partial\vec{v}/\partial t)+U_n(\partial\vec{v}/\partial x)=0$, where U_n is the normal outflow velocity at the boundary.

For *Re=40*, the Euler implicit method is used with $Dt=0.5$. The L2 norm of the steady state residual in Eq. (2) dropped 5 orders of magnitude in 250 steps. The computed pressure coefficient contours and the streamlines are plotted in Fig. (1). Note

Advances in Computational & Experimental Engineering & Science

that the pressure inside the cylinder adjusts automatically to follow the pressure field outside. The smoothness of the streamlines around the cylinder indicates that Eq. (5) is satisfactory in treating the cylinder geometry in our case. Table I lists the computed lift *(Cl)* and drag *(Cd)* coefficients and the wake length normalized by the diameter *(Lw/d)*.

For *Re=200*, the second order backward difference scheme with $Dt = 0.1$ is used. The instantaneous pressure coefficient contours and streamlines at *t=300* are plotted in Fig. (2). Again, note the pressure inside the cylinder varies automatically according to the pressure outside. The streamlines show the unsteady vortex shedding behind the cylinder. The computed aerodynamic coefficients and Strouhal number based on the lift coefficient are listed in Table I. The comparison with the work of others is satisfactory.

Table I Simulation Results for Flow over a Circular Cylinder

Methods	*Re*	*Cd*	*Lw/d*	*D Cl*	*St*
Current	*40*	*1.53*	*2.13*		
	200	1.32 ± 0.043		± 0.62	*0.198*
Ye et al.[3]	*40*	*1.52*	*2.27*		
Kiris and Kwak [8]	*200*	1.27 ± 0.04		± 0.67	*0.184*

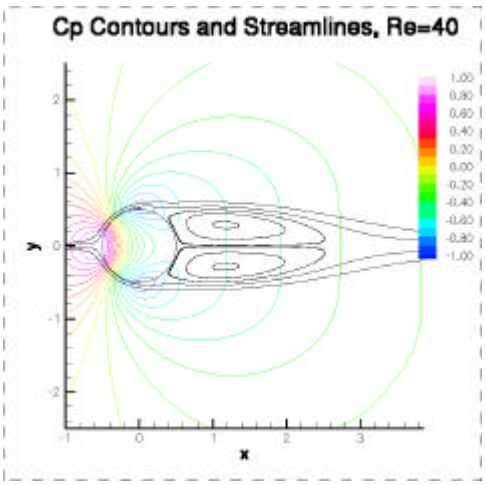

Fig. (1) Re=40, Cp and Streamlines

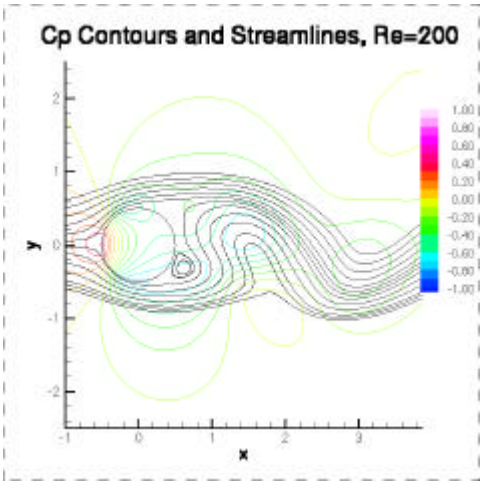

Fig. (2) Re=200, Cp and Streamlines

Flow over a Flapping Ellipse

In Fig. (3), an ellipse is in a forced "figure-8" motion. The down-stroke phase is plotted in black while the up-stroke phase is in red. As described in Wang [9], a "figure-8" motion is used to simulate the flapping motion of an insect wing. The movement of the center of the ellipse is governed by $A(t) = 0.5A_0 [\cos(2pt / T)]$, where T is the

Advances in Computational & Experimental Engineering & Science

flapping period and A_0 is the amplitude. The stoke plane along which the center moves has an inclination angle b with respect to the horizontal axis. The angle of attack is governed by $0.25p[1-\sin(2pt/T+j)]$, where j is a phase lag. In our choice, the reference speed is *400cm/s*, the reference length is *4cm*, the major axis of the ellipse is *1cm*, and the kinematic viscosity is $2cm^2/s$. The flapping motion has $b=60^\circ$, A_0=*2.5cm*, *T=0.025sec* and $j=0$. The Reynolds number amounts to *Re=800*. The time increment is set to *1/400 T*. The outer boundary of the grid is *40cm* in length. The grid is refined in the region where the figure-8 motion occurs. The volume of the ellipse computed by function f_B is about *0.25%* lower than the analytical value.

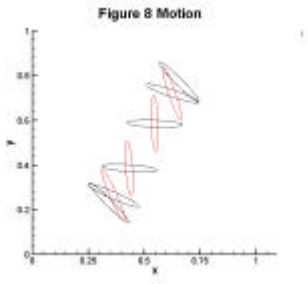

Fig. (3) "Figure-8" motion.

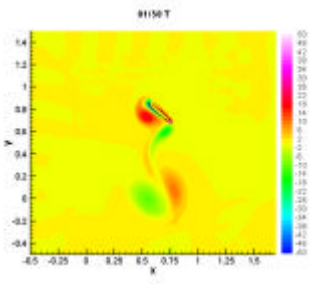

Fig. (4a) t=(1/50)T, Vorticity

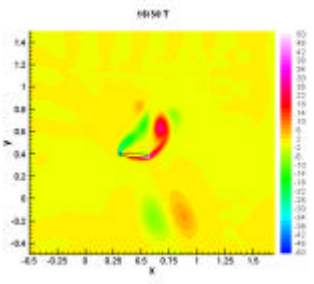

(4b) t=(16/50)T

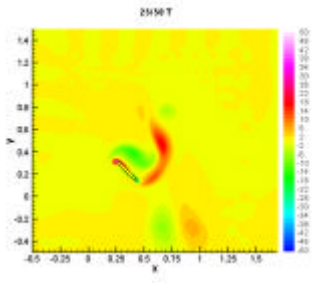

(4c) t=(25/50)T

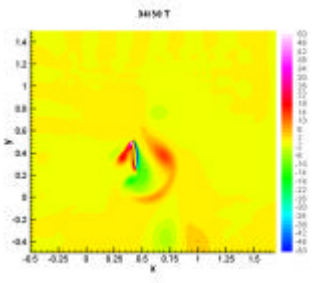

(4d) t=(34/50)T,

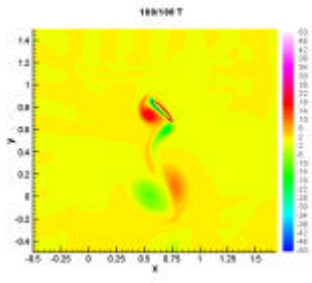

(4e) t=(50/50)T

Figures (4a) to (4e) show the vorticity contours in sequence. The vorticity generation along the body surface and the vortex shedding at the two tips are clearly seen. During the down-stroke phase, a pair of counter-rotating vortices is generated by the downward translation and rotation of the ellipse. During the up-stroke phase, the upward translation and rotation of the body fuses the leading and trailing edge vortices to form a dipole vortex pair, moving downward with the "jet stream" flowing away from the body. This downward jet stream is responsible for the generation of lift and thrust on the body. Compare with the vortex generation process of an elliptical airfoil in the Fig. 2 of Wang [9], the basic vortex dynamics are qualitatively similar.

Advances in Computational & Experimental Engineering & Science

Conclusions

A simple and effective model for the immersed bodies in incompressible flows has been implemented in an implicit fractional step pressure correction method. The domain of the solid body is treated as being occupied by the same fluid as outside with a prescribed divergence-free velocity. The pressure field inside the body is computed by the same Poisson equation used for the fluid flow outside. The velocity of the interface cell is a volume-averaged mixture of the body velocity and the velocity estimated by the conservation equations. The computations of steady and unsteady flows over a circular cylinder show good comparison with the work of others. Preliminary results of the flow over an ellipse in a forced "figure-8" motion are shown to demonstrate the capability of the present method to treat large and complex body movements.

Acknowledgements

This work is funded by National Science Council under the grants NSC91-2212-E006-104 and NSC92-2212-E006-105. The support is highly appreciated.

References

1 Peskin, C. S. (2002): "The Immersed Boundary Method", *Acta Numerica*, pp. 1-39.

2 Goldstein, D., Handler, R. and Sirovich, L. (1993): "Modeling a No-Slip flow Boundary with an External Force Field", , *J. Comput. Phys*., Vol. 105, pp. 354-366.

3 Ye, T., Mittal, R., Udaykumar, H.S. and Shyy, W. (1999): "An Accurate Cartesian Grid Method for Viscous Incompressible Flows with Complex Immersed Boundaries", *J. Comput. Phys*., Vol. 156, pp. 209-240.

4 Fadlun, E.A., Verzicco, R., Orlandi, P. and Mohd-Yusof, J. (2000): "Combined Immersed-Boundary Finite-Difference Methods for Three-Dimensional Complex Flow Simulations", *J. Comput. Phys*, Vol. 161, pp. 35-60.

5 Kim, J., Kim, D., and Choi, H. (2001): "An Immersed-Boundary Finite-Volume Method for Simulations of Flow in Complex Geometries", *J. Comput. Phys.*, Vol. 171, pp. 132-150.

6 Pan, D. (2003): "An Implicit Pressure Correction Method for Incompressible Navier-Stokes Equations on Unstructured Cartesian Grids", Proceedings of the 5th Asian Computational Fluid Dynamics Conference, Busan, Korea, Oct. 27-30.

7 Pan, D. (2003): "Incompressible Navier-Stokes Simulation of Two-Dimensional Plate in Large Amplitude Flapping Motion", Proceedings of the 10th National Computational Fluid Dynamics Conference, Hua-Lian, Taiwan ROC, August 23-25.

8 Kiris, C. and Kwak, D. (2001): "Numerical Solution of Incompressible Navier-Stokes Equations Using a Fractional-Step Approach", *Comp. & Flu.*, Vol. 30, pp. 829-851.

9 Wang, Z.J. (2000): "Two dimensional Mechanism for Insect Hovering", *Physical Review Letters*, Vol. 85, No. 10, Sept. 4, pp. 2216-2219.